AIAA JOURNAL
Vol. 48, No. 8, August 2010

Turbulence Modeling for Low-Reynolds-Number Flows

P. Catalano*
Italian Aerospace Research Center, 81043 Capua, Italy
and
R. Tognaccini†
University of Naples "Federico II", 80125 Naples, Italy

DOI: 10.2514/1.J050067

A modification of the κ-ω shear-stress-transport turbulence model is presented in this paper with the aim to improve the simulation of flows at a low Reynolds number. For this purpose, the incompressible flow at Reynolds number 6×10^4, around the Selig–Donovan 7003 airfoil, is investigated by using several turbulence models. The focus is placed on the κ-ω shear-stress-transport turbulence model: a model very reliable for transonic flows but for which the application to low-Reynolds-number flows has been questioned. The limits of this model are analyzed in detail. The simulation of the laminar bubble arising on the SD 7003 airfoil has been remarkably improved by the proposed modification. In addition, the accuracy of the κ-ω shear-stress-transport turbulence model has been preserved in the transonic regime at a high Reynolds number, as shown by the simulations of the flow around the RAE M2155 wing. Large-eddy simulations of the flow around the Selig–Donovan 7003 airfoil have also been performed and presented in the paper. The large-eddy-simulation data are used as a reference for the results achieved by the Reynolds-averaged Navier–Stokes method. The computed aerodynamic coefficients are compared with some available experimental data.

Nomenclature

a_1	=	constant in the Reynolds shear stress formula
B	=	constant in the logarithmic law of the velocity
b	=	wing span
C_D	=	drag coefficient
C_F	=	friction coefficient
C_L	=	lift coefficient
C_P	=	pressure coefficient
c	=	airfoil chord
g	=	$1/(\beta^*\omega)$
L	=	length
N_{crit}	=	critical amplification parameter
Re	=	Reynolds number
t	=	time
u, v, w	=	velocity components in x, y, and z directions
u_j	=	velocity in tensor notation
u_τ	=	friction velocity
V	=	module of the velocity
x, y, z	=	Cartesian coordinates
x_j	=	position vector in tensor notation
y^+	=	distance from the surface in viscous units
α	=	angle of attack
$\beta, \beta^*, \gamma, \sigma_\kappa$	=	closure coefficients
ϵ	=	turbulent dissipation rate
κ	=	turbulent kinetic energy
κ_a	=	von Kármán constant
μ	=	molecular viscosity
μ_t	=	eddy viscosity
ν	=	kinematic viscosity, $\frac{\mu}{\rho}$
$\tilde{\nu}$	=	working variable of the Spalart–Allmaras turbulence model
ρ	=	density
$\sigma_\omega, \sigma_{\omega_2}$	=	closure coefficients
τ	=	Reynolds shear stress
τ_{ij}	=	Reynolds stress tensor
Ω	=	vorticity
ω	=	specific dissipation rate, $\varepsilon/(\beta^*\kappa)$

Subscripts

ref	=	reference
tr	=	transition
∞	=	freestream conditions

Superscript

$+$	=	viscous units

Received 15 July 2009; revision received 27 November 2009; accepted for publication 16 January 2010.

*Research Engineer, Department of Physics of Fluids. Member AIAA.
†Associate Professor, Department of Aerospace Engineering. Senior Member AIAA.

I. Introduction

THE growing interest of the aerospace industries in unmanned and micro aerial vehicles (UAVs and MAVs) is pushing the research in the field of the low-Reynolds number flows. UAV wings typically operate at a Reynolds number of 10^4–10^5. At these Reynolds numbers, the flow cannot sustain strong adverse pressure gradients and often separates in the laminar regime. The turbulence developing inside the recirculation region enhances the momentum transport, and the flow reattaches. This phenomenon, the laminar separation bubble (LSB), is one of the main critical aspects of low-Reynolds-number flows.

The only simulation techniques feasible to be applied to complex configurations, such as high-altitude long-endurance unmanned vehicles, appear to be the methods based on the Reynolds-averaged Navier–Stokes (RANS) equations. A critical point in applying the RANS approach to low-Reynolds-number flows is the turbulence modeling. In fact, the presence of separation bubbles means that the separation is laminar and that the transition points are very difficult to set. The turbulence models are instead calibrated for separation in the turbulent flow regime, and they need the transition points to be known a priori.

The possibility of using the RANS equations for the numerical simulation of low-Reynolds-number flows and LSBs is addressed in several papers. Howard et al. [1] performed RANS simulations of a laminar bubble over a flat plate, using the κ-g model [2], with and without fixing the transition point and modified by using coefficients,

depending on the local turbulent Reynolds number as proposed by Wilcox [3]. The model without any treatment of the transition provides a very weak separation. The model with modified coefficients presents a bubble with a reattachment anticipated with respect to direct numerical simulation (DNS). The κ-g model not modified, but applied with the transition point imposed, returns a bubble. The reattachment point is located more downstream than the DNS data.

The RANS approach, with some treatment to take into account the transition phenomenon, has been applied to the Selig–Donovan (SD) 7003 airfoil by several researchers. This airfoil exhibits a laminar bubble over a broad range of incidences, and it has been the subject of numerical and experimental [4] investigations. Windte et al. [5], Radespiel et al. [6], and Yuan et al. [7] employed a RANS solver coupled to a transition prediction method to simulate the flow around the SD 7003 airfoil at $Re = 6 \times 10^4$. Comparison between the contour plots of experimental and computed shear stress is presented. Pressure and friction coefficients obtained by large-eddy simulation (LES) and RANS are shown. The best results are achieved by the Menter baseline (BSL) two-layer model [8], the explicit algebraic Reynolds stress model (RSM) by Wallin and Johansson [9], and the Wilcox RSM [3]. The drag polar of the airfoil is computed with a reasonable accuracy. A systematic overprediction of the C_L with respect to the experiments is, however, noted. Some dependence of the results on the choice of the N_{crit} is seen mainly at high incidences.

An easier approach has also been tried. Tang [10] applied the RANS equations without any particular treatment of the transition to the flow at $Re = 6 \times 10^4$, around the SD 7003 airfoil. First, a laminar simulation is performed. The transition is considered to occur in the separated region at the point where the flow reverses direction and moves downstream. Then, a simulation with an imposed transition point is performed. Results are presented for the flow at $\alpha = 4^\circ$ in terms of the contour plot of the Reynolds stresses, pressure coefficient, and velocity contours with streamlines. Good results are achieved by the Spalart–Allmaras model. A too-short bubble is instead returned by the Menter BSL two-layer [8] and the Jones and Launder [11] κ-ε models.

The LESs of low-Reynolds-number flows are becoming affordable, at least for validating the results of the much faster RANS solvers. Indeed, LESs of the flow around the SD 7003 airfoil have been performed. Yuan et al. [7] employed an incompressible solver, using the SIMPLE algorithm [12] for the pressure–velocity coupling. The static Smagorinsky and the selective scale model by Lenormand et al. [13] have been used as subgrid closures of the Navier–Stokes equations. The flow at $Re = 6 \times 10^4$ and $\alpha = 4^\circ$ has been computed. Difference with respect to RANS results in the zone of the bubble in terms of pressure and friction coefficients are shown. The importance of three-dimensional fluid structures is discussed. Galbraith and Visbal [14] applied a high-order implicit LES to compute the entire drag polar of the SD 7003 airfoil at $Re = 6 \times 10^4$. Good accuracy with the experimental data is shown. The stall is well predicted. The C_L also compares well with the experiments at a poststall angle, while the C_D is overpredicted.

Rumsey and Spalart [15] have performed an analysis of the behavior of the Spalart–Allmaras and the κ-ω shear-stress-transport (SST) (modified adding sustaining terms [16]) turbulence models in low-Reynolds-number regions of an aerodynamic flowfield. They tested the behavior of the models over a flat plate with decreasing values of the freestream turbulence, and they found that the κ-ω SST exhibits a correct trend for the transition to turbulence. Catalano and Tognaccini [17] have performed a similar analysis. Both the Spalart–Allmaras and the κ-ω SST provide a jump from the Blasius laminar to the Prandtl turbulent curve of the friction coefficient. The jump occurs at a higher Reynolds number as the freestream turbulence decreases for the Spalart–Allmaras. The κ-ω SST shows a sort of convergence as the freestream turbulence is lowered, with the jump occurring at $Re \approx 1 \times 10^5$. Rumsey and Spalart [15] also considered the flow around the NACA 0012 airfoil at Reynolds number 1×10^5. The main conclusion of their article was "these models are intended for fully turbulent high-Reynolds-number computations and using them for transitional (e.g., low Reynolds number) or relaminarizing flows is not appropriate. Competing models which fare better in these areas have not been identified."

The aim of this paper is to give a contribution to the turbulence modeling of low-Reynolds-number flows. A RANS method is applied by using several turbulence models to the incompressible flow at Reynolds number 6×10^4 around the SD 7003 airfoil. The results are analyzed adopting LESs of the same flow as reference. The focus is placed on the κ-ω SST turbulence model; a model that, despite of the limits shown in low-Reynolds-number applications, is very reliable for transonic flows, as pointed out by different authors (cf., Catalano and Amato [18]).

The limits of this model have been confirmed. However, it is shown that they are not due to design problems of the model but rather to its implementation. Indeed, a modification of the SST formulation is proposed here. It allows for a very satisfactory simulation of the LSB when the transition point is prescribed. An excellent agreement with the LES results is obtained in terms of pressure and skin friction distributions along the SD 7003 airfoil.

In addition, the performance of the model is not reduced in the transonic regime at a high Reynolds number, as shown by computing the flow around the RAE M2155 wing.

II. Numerical Methods

The results discussed in this paper have been achieved by a numerical method based on the RANS equations and by LESs.

A. Reynolds-Averaged Navier–Stokes Solver

The flow solver adopted is a multiblock zonal Euler/RANS well-assessed tool for the analysis of complex configurations in the subsonic, transonic, and supersonic regimes [18]. The equations are discretized by means of a standard cell-centered finite-volume scheme with blended self-adaptive second- and fourth-order artificial dissipation. The pseudotime-marching advancement is performed by using the Runge–Kutta algorithm with convergence accelerators, such as the multigrid and residual smoothing techniques. A time-accurate version of the flow solver has also been developed [19]. The time integration is based on the dual-time stepping method [20], where a pseudosteady-state problem is solved at each physical time step.

The turbulence equations are weakly coupled with the RANS equations and solved only on the finest grid level of a multigrid cycle. Algebraic, one-equation, two-equation [21], and nonlinear eddy viscosity turbulence models [22] are available.

The focus of the paper is on the κ-ω SST turbulence model. To simplify the discussion, it is useful to recall the equations and the formulas as proposed in the original paper by Menter [8]. The equations of this model read as

$$\frac{\partial(\rho\kappa)}{\partial t} + \frac{\partial(\rho\kappa u_j)}{\partial x_j} = \tau_{ij}\frac{\partial u_i}{\partial x_j} - \beta^*\rho\omega\kappa + \frac{\partial}{\partial x_j}\left[(\mu + \sigma_k\mu_t)\frac{\partial\kappa}{\partial x_j}\right] \tag{1}$$

$$\frac{\partial(\rho\omega)}{\partial t} + \frac{\partial(\rho\omega u_j)}{\partial x_j} = \gamma\frac{\rho}{\mu_t}\tau_{ij}\frac{\partial u_i}{\partial x_j} - \beta\rho\omega^2 + \frac{\partial}{\partial x_j}\left[(\mu + \sigma_\omega\mu_t)\frac{\partial\omega}{\partial x_j}\right] + 2(1 - F_1)\rho\sigma_{\omega_2}\frac{1}{\omega}\frac{\partial\kappa}{\partial x_j}\frac{\partial\omega}{\partial x_j} \tag{2}$$

where β^*, β, γ, σ_κ, σ_ω, and σ_{ω_2} are constants, and τ_{ij} is the Reynolds stress tensor; $i, j = 1, 2, 3$, and the convention on the repeated index summation is assumed. The blending function F_1 allows a switch from a κ-ω-type model close to a solid boundary to a κ-ε-type model in the outer part of the boundary layer.

The SST formulation accounts for computing the shear stress as

$$\tau = a_1\kappa \tag{3}$$

in a suitable part of the boundary layer. This is obtained by considering that

$$\tau \approx \mu_t \Omega \tag{4}$$

where Ω is the vorticity. The eddy viscosity is computed by making use of a switching between the specific turbulent dissipation ω and Ω:

$$\mu_t = \frac{\rho a_1 \kappa}{\max(a_1 \omega, F_2 \Omega)} \tag{5}$$

where $a_1 = 0.3$, and F_2 is a blending function computed as

$$F_2 = \tanh(\mathrm{Arg}2^2) \tag{6}$$

where

$$\mathrm{Arg}\,2 = \max(\mathrm{Arg}21, \mathrm{Arg}22) \tag{7}$$

with

$$\mathrm{Arg}\,21 = \frac{2\sqrt{\kappa}}{\beta^* \omega y}; \qquad \mathrm{Arg}22 = \frac{500\mu}{\omega y^2} \tag{8}$$

The function F_2 has been designed to be one close to solid boundaries and zero in the upper part of the logarithmic region of a turbulent boundary layer, where Eq. (3) should be recovered.

B. Large-Eddy-Simulation Solver

An incompressible flow solver of the Navier–Stokes equations is used for the LES. The code employs an energy-conservative numerical scheme. Second-order central differences in streamwise and wall-normal directions and Fourier collocations in the spanwise direction are used. The code is written in body-fitted coordinates, with a staggered arrangement of the flow variables. The fractional step approach [23], in combination with the Crank–Nicholson method for the viscous terms and the third-order Runge–Kutta scheme, is used for the time advancement. The continuity constraint is imposed at each Runge–Kutta substep by solving a Poisson equation for the pressure. The subgrid-scale stress tensor is modeled by the dynamic Smagorinsky model [24] in combination with a least-contraction and spanwise averaging [25].

III. Results by the κ-ω Shear-Stress-Transport Turbulence Model

Simulations of flows at a low Reynolds number achieved by the standard κ-ω SST turbulence model are discussed in this section. The incompressible flow around the SD 7003 airfoil at a Reynolds number of 6.0×10^4 is taken into consideration. This is a widely used test case for which experimental [4] and numerical [14] data are available in literature. RANS and LESs at several angles of incidence have been performed. The main aim is to analyze the limits of the RANS methods by comparison with LES results. The NEC SX6 machine has been used. A RANS simulation has been obtained in about 8 h, while a LES solution has required about 30 days CPU of a single processor.

Flows at a low Reynolds number are not able to sustain strong adverse pressure gradients and often separate in the laminar flow regime. The turbulence developing inside the recirculation region enhances the momentum transport, and the flow reattaches. The presence in the flowfield of LSBs means that the transition points cannot be set a priori. This is a critical point for the turbulence models that are calibrated for separation in the turbulent flow regime and need the transition points to be known.

A first set of results has been obtained by running the turbulence models without specifying the transition points (flows are assumed turbulent everywhere). LSBs are detected if the turbulence models are robust enough to be run with very low values of freestream turbulence. Another set of results are presented by running the turbulence model with the transition location fixed at a point retrieved by the LES data.

A. Grid Assessment

A C-topology grid with 768 (96 in the wake) cells in the streamwise and 176 cells in the normalwise direction has been employed. The far-field boundaries are located at a distance of 30 chords from the airfoil. The height of the wall-adjacent cells in the wall-units coordinate remains less than one for all of the upper surface of the airfoil.

The two-dimensional mesh of the RANS computations has also been employed for the LESs. The only difference is that the branch-cut line is adapted to follow the wake with the angle of attack. The spanwise extension of the computational domain is $0.1 \times c$ with 48 cells. The wall-adjacent cells in the wall-units coordinate have a size of less than one in the wall-normal direction and on order of magnitude of 10 in the streamwise and spanwise directions.

A grid convergence study (Fig. 1) has been performed for the RANS solutions. Five levels of the computational mesh are considered. The two coarsest grids provide a separated flow. The flow reattaches in the three finer meshes, with the reattachment point between 50 and 60% of the chord. Differences between the fourth and fifth levels of the grid are negligible for both the pressure (Fig. 1a) and friction coefficients (Fig. 1b). Therefore, the results obtained on the grid with 768×176 cells are considered sufficiently accurate.

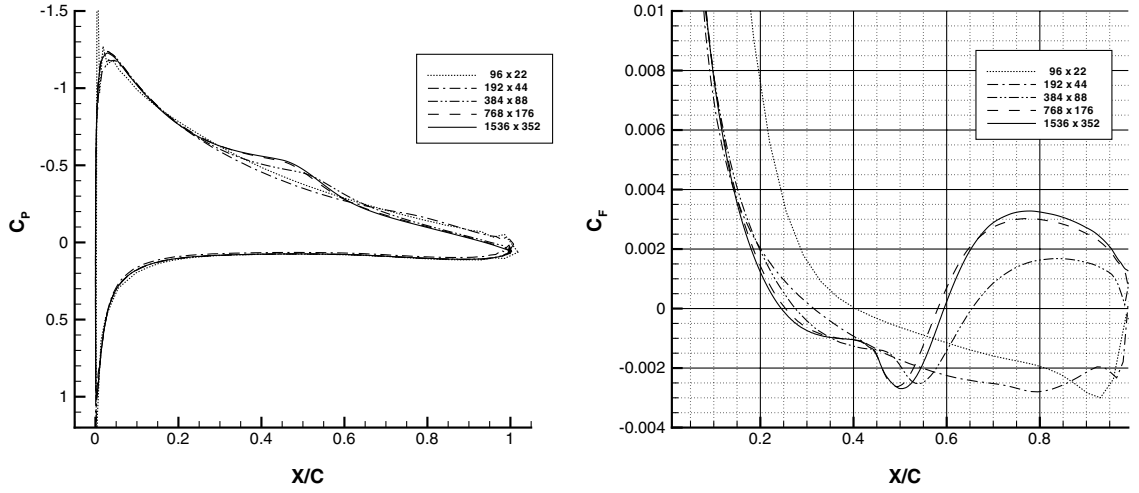

a) Pressure coefficient **b) Friction coefficient**

Fig. 1 SD 7003 airfoil, $Re = 6.0 \times 10^4$, $\alpha = 4°$. Grid convergence study of the RANS solution.

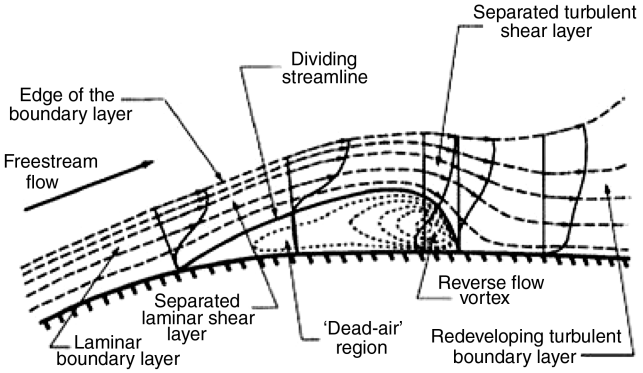

Fig. 2 Structure of a LSB, from Horton [27].

B. Analysis of Laminar Separation Bubbles

The capability of the RANS models to predict a LSB is discussed in this section. A sketch of the typical structure of a LSB is shown in Fig. 2. A large part of the separated zone is characterized by a slow flow motion. This is named as the dead-air region. The last part of the bubble presents a stronger recirculation vortex flow. Looking at the path of the dividing streamline, it is clear that a sudden pressure recovery leading to the reattachment of the flow occurs in this zone.

The authors have computed the laminar bubble over a flat plate with imposed pressure gradients [17]. Simulations with and without the transition location prescribed were performed. The effect of decreasing the values of the freestream turbulence was assessed when the models were used without imposing the transition. The results achieved by the κ-ω SST, with $(\mu_t/\mu)_\infty = 1 \times 10^{-9}$ and $(\sqrt{\kappa}/U)_\infty = 10^{-6}$, and by the Spalart–Allmaras, with $(\tilde{\nu}/\nu)|_\infty = 10^{-15}$, resemble the data obtained by prescribing the transition and reproduce a DNS solution quite well in the laminar region of the flow.

These two models, used with low values of freestream turbulence, have also shown a sort of numerical transition for the flow without pressure gradient over a flat plate. Rumsey and Spalart [15] have obtained similar results for the κ-ω SST model.

The flow around the SD 7003 airfoil at a Reynolds number of 6×10^4 presents a laminar bubble that moves from the trailing to the leading edge as the angle of attack increases.

RANS simulations of the flow at $Re = 6 \times 10^4$ and $\alpha = 4°$ around the SD 7003 airfoil have been performed by using several turbulence models. The transition is not specified, and the flow is assumed to be turbulent everywhere. The Spalart–Allmaras, the κ-ε Myong–Kasagi (MK), and the κ-ω Wilcox [3] turbulent nonturbulent (TNT) [26], BSL, and SST [8] are the models tested. The freestream values used for the κ-ω TNT, BSL, and SST, and the Spalart–Allmaras models are the same as those employed for the laminar bubble over the flat plate. Instead, the κ-ω Wilcox and the κ-ε MK have shown to be less robust, and the value of the freestream turbulence is decreased, provided that a converged solution can be achieved.

The LESs by the authors and by Galbraith and Visbal [14] are taken as reference data.

All the RANS results show a different solution in terms of pressure (Figs. 3a and 3c) and friction coefficients (Figs. 3b and 3d)

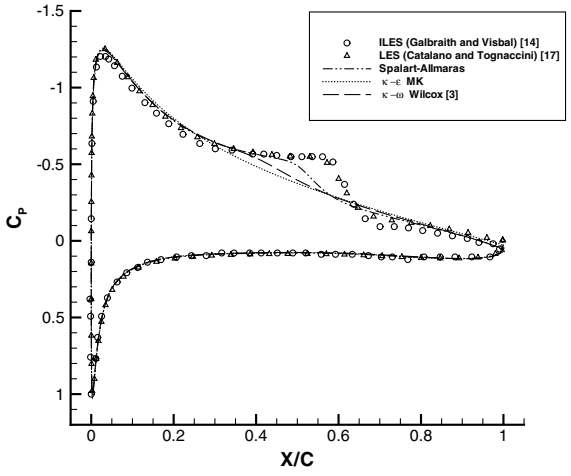

a) Pressure coefficient

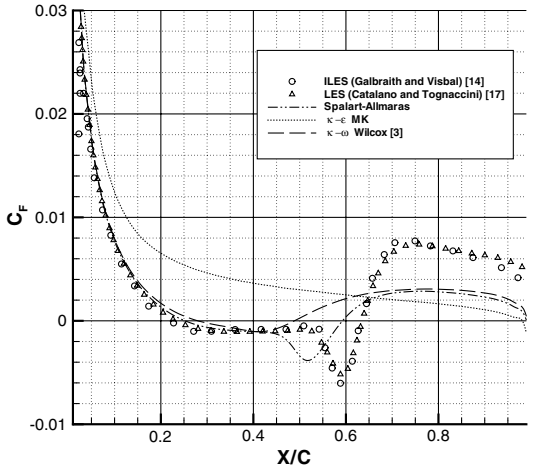

b) Friction coefficient

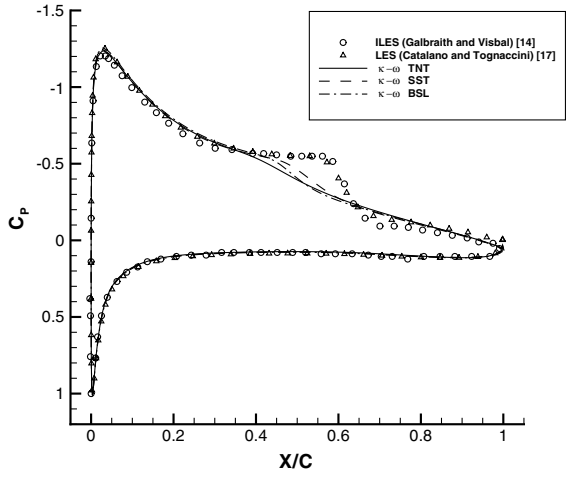

c) Pressure coefficient

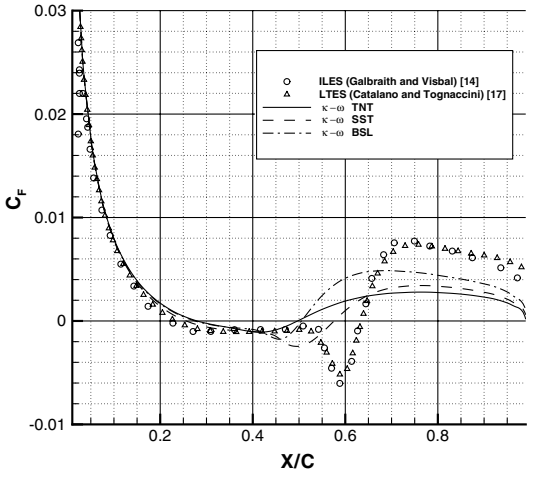

d) Friction coefficient

Fig. 3 SD 7003 airfoil, $Re = 6.0 \times 10^4$, $\alpha = 4°$. Results by several turbulence models.

with respect to LES. The differences are better appreciated when looking at the friction coefficient on the upper surface. The κ-ε does not provide a flow separation. A flow with a separation and a reattachment is returned by all the other turbulence models. The κ-ω SST and the Spalart–Allmaras provide a qualitatively good result. The friction coefficient presents a flat zone followed by a decrease. Downstream of the minimum of C_F, a pressure recovery occurs, and the flow reattaches. The same behavior is shown by the LES data. The κ-ω BSL yields a result in between the TNT and SST models.

In the following, the focus is placed on the κ-ω SST turbulence model. This model is very popular and reliable for transonic high-Reynolds-number flows, as pointed out by different authors (cf., Catalano and Amato [18]), but its effectiveness for low-Reynolds-number flows is doubtful (Catalano and Tognaccini [17] and Rumsey and Spalart [15]).

Several angles of incidence are taken into consideration, and the κ-ω SST model is applied with $(\mu_t/\mu)_\infty = 1 \times 10^{-9}$ and $(\sqrt{\kappa}/U)_\infty = 10^{-6}$. A boundary layer with negligible values of the eddy viscosity develops from the stagnation point, implying (in practice) a laminar evolution of the flow ahead of the separation. The friction and pressure coefficients as a function of the angle of attack are presented in Fig. 4. A bubble is predicted in the trailing-edge zone of the airfoil at $\alpha = 0°$ and then moves toward the leading edge as α increases.

A comparison between the bubble returned by the RANS and LES methods at $\alpha = 4°$ is presented in Fig. 5. The streamlines with the contour map of the module of the velocity and the pressure coefficient in the zone of the bubble are presented. The LES results are averaged along the span direction and in time for about eight characteristic times. The structure of a LSB [27] (Fig. 2) can be recognized. A dead-air region is returned by both RANS and LES. The zone of reverse flow lying below the dividing streamline is characterized by a very low value of the V/V_∞ for a large extent of the bubble. The pressure recovery occurs in the zone where stronger negative velocities are attained by the flow. A reverse flow vortex is seen in the LES results, while a more spread region of pressure recovery is returned by the RANS method.

The RANS solutions, in terms of pressure and friction coefficients, are compared with the LES data by the authors and Galbraith and Visbal [14] in Figs. 3c and 3d at $\alpha = 4°$ and in Figs. 6 and 7 at $\alpha = 6$, and 8°, respectively. The pressure recovery in the zone of the bubble is much stronger in LES than in RANS data, as can be seen in all the C_P and C_F plots. The separation point is well predicted in the RANS simulations, but the RANS provide a reattachment anticipated with respect to LES results. Downstream of the flow reattachment, the RANS recover to a level of pressure lower than LES. Incidentally, the present LESs are in excellent agreement with the implicit LES (ILES) by Galbraith and Visbal [14], except for the case $\alpha = 6°$.

The RANS simulations have been performed without an a priori knowledge of the laminar-turbulent transition. It has been shown that a laminar bubble is returned by the RANS methods, with the κ-ω SST and the Spalart–Allmaras turbulence models used with low values of freestream turbulence. The RANS satisfactorily predicts the separation point and the flow in the dead-air region. A shorter bubble length and a weaker pressure recovery is provided by RANS with respect to LES.

For $\alpha = 4°$, the flow has also been computed by imposing the transition location at $x_{tr}/c = 0.53$, a value retrieved by LES data. The production terms of the turbulence equations are set to zero in the prescribed laminar regions. The results are expected to improve when the turbulence models are run, with the transition point fixed at a reasonable location. This is shown in literature and has been verified by the authors [17] for the flow over a flat plate with an imposed pressure gradient [28,29].

The κ-ω BSL and SST turbulence models [8] are applied. The comparison between the friction and pressure coefficients, achieved by applying the two models without and with the transition location fixed a priori, is shown in Fig. 8. The two κ-ω models provide a similar result when used without fixing the transition location. On the contrary, a large difference occurs when the simulations are performed with the transition point fixed a priori. The κ-ω BSL provides a pressure recovery closer to the LES data. On the contrary, the κ-ω SST produces a too-low turbulence, and the flow does not reattach.

The SST formulation should allow for a better characterization of flow separations and reattachments. This has been verified for typical transonic benchmarks but, as shown by the present results, at a low Reynolds number seems to provide results even worse than the BSL model. This confirms the analysis performed by Rumsey and Spalart [15] on the poor accuracy of the κ-ω SST for low-Reynolds-number flows.

C. Analysis of Shear-Stress-Transport Formulation for Low-Reynolds-Number Flows

The SST formulation has been designed in order to recover Eq. (3) in the upper part of the logarithmic region of a boundary layer. The presence and extension of the logarithmic region depends on the Reynolds number. In particular, its extension increases as the Reynolds number increases.

The flow around the SD 7003 airfoil has been analyzed at $\alpha = 0°$ and Reynolds numbers 6.0×10^6, 6.0×10^5, and 6.0×10^4. The turbulent intensity has been set to 0.1%, and the ratio between the freestream turbulent and molecular viscosity has been set to 0.1. This numerical setting allows one to concentrate on the effect of the Reynolds number on the boundary-layer velocity profile, because

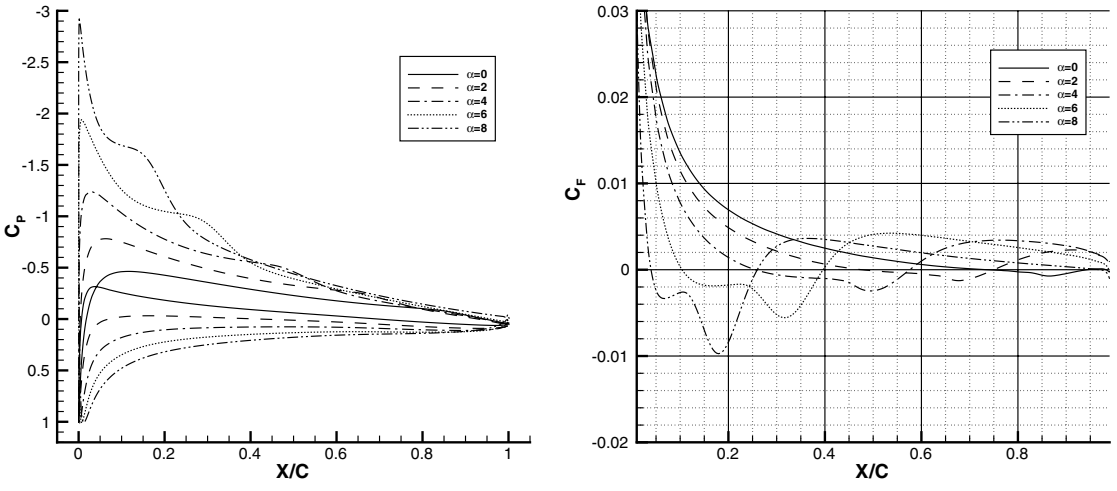

a) Pressure coefficient **b) Friction coefficient**

Fig. 4 SD 7003 airfoil, $Re = 6.0 \times 10^4$. RANS, κ-ω SST with laminar-turbulent transition not prescribed: C_P and C_F over the airfoil at different angles of attack.

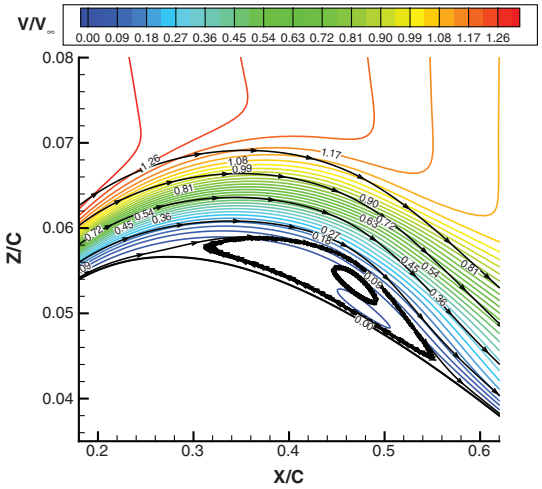

a) RANS, $\kappa-\omega$ SST with laminar-turbulent transition not prescribed: streamlines and contour map of the module of the velocity

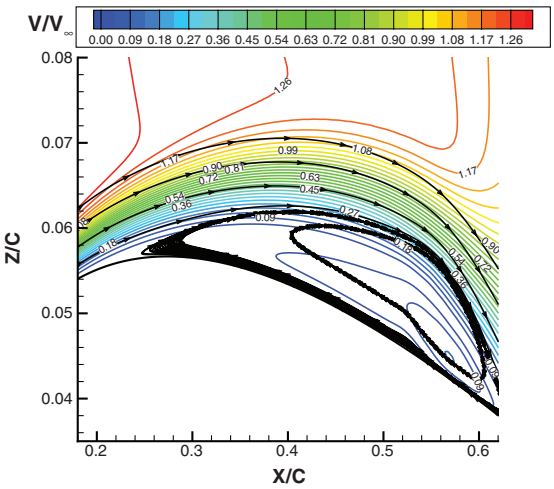

b) LES: streamlines and contour map of the module of the velocity

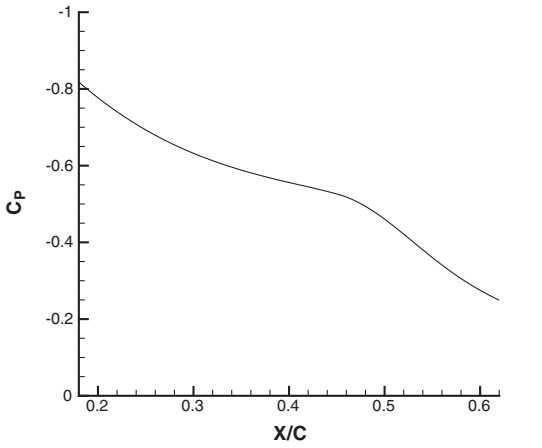

c) RANS, $\kappa-\omega$ SST with laminar-turbulent transition not prescribed: pressure coefficient in the zone of the bubble

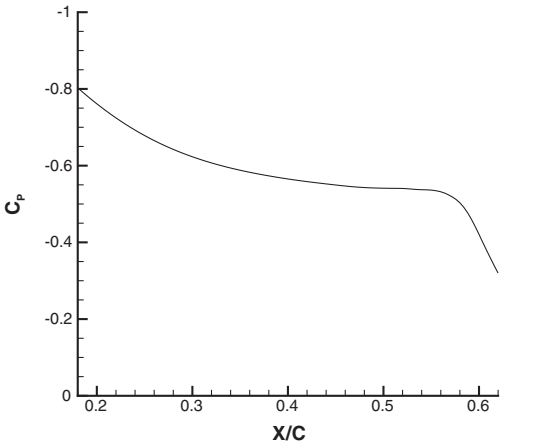

d) LES: pressure coefficient in the zone of the bubble

Fig. 5 SD 7003 airfoil, $Re = 6.0 \times 10^4$, $\alpha = 4°$. Structure of the laminar bubble.

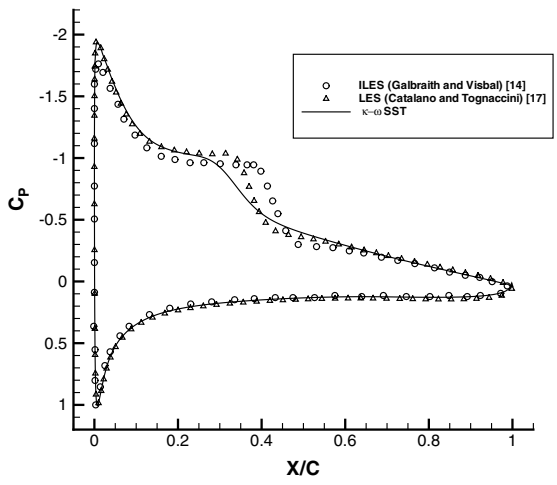

a) Pressure coefficient

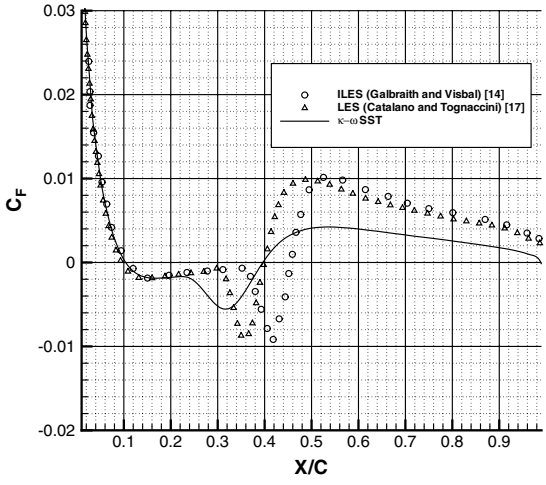

b) Friction coefficient

Fig. 6 SD 7003 airfoil, $Re = 6.0 \times 10^4$, $\alpha = 6°$. Pressure and friction coefficient.

LSBs are not returned by any of the simulations. The spacing of the first layers of cells has been adapted to the Reynolds number in such a way as to obtain a y^+ of an order of magnitude of one for all the simulations.

The streamwise velocity profiles have been analyzed at several stations along the upper surface of the SD 7003 airfoil. The results at the representative station $X/C = 0.90$ are shown in Fig. 9. The curves $u^+ = y^+$ corresponding to the viscous sublayer, and $u^+ =$

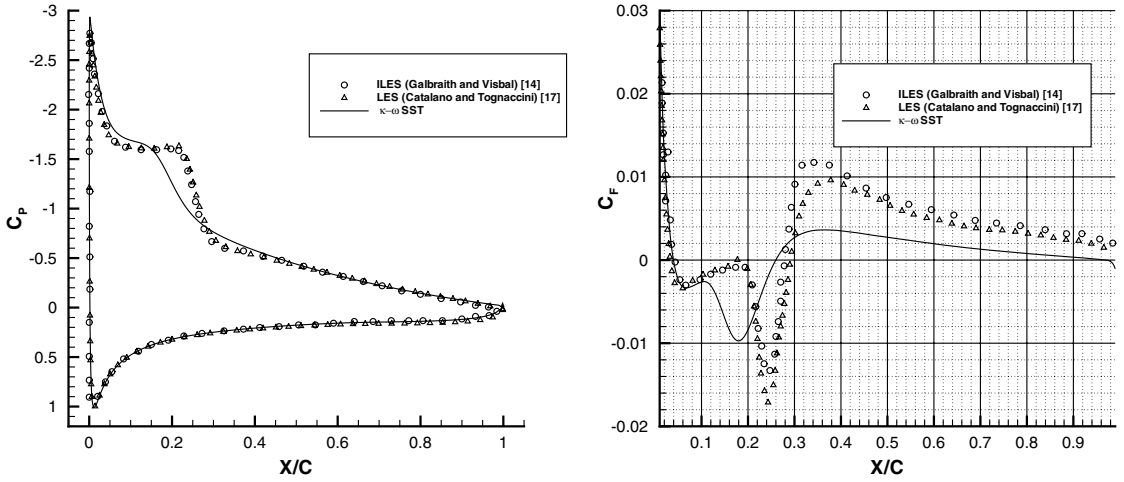

a) Pressure coefficient b) Friction coefficient

Fig. 7 SD 7003 Airfoil, $Re = 6.0 \times 10^4$, $\alpha = 8°$. Pressure and friction coefficient.

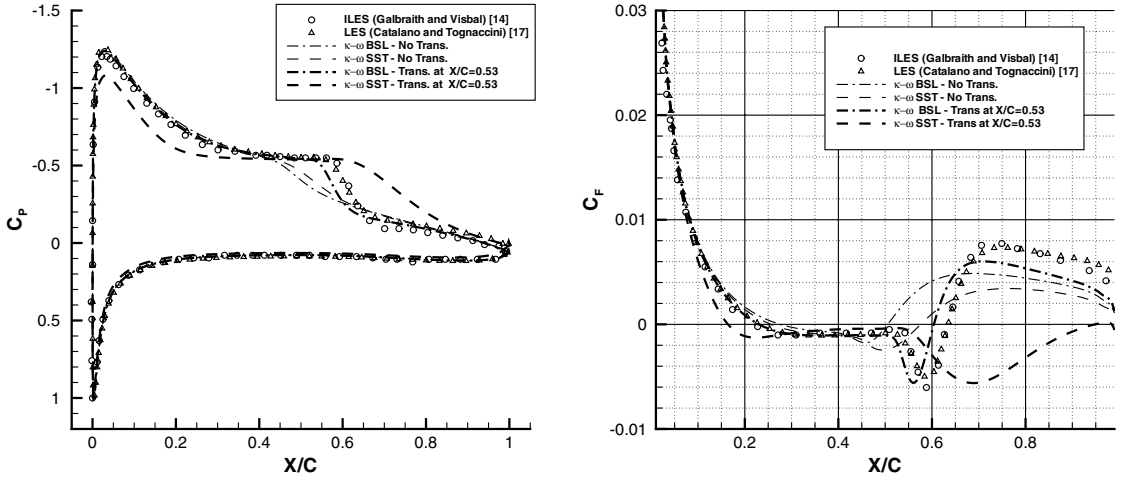

a) Pressure coefficient b) Friction coefficient

Fig. 8 SD 7003 Airfoil, $Re = 6.0 \times 10^4$, $\alpha = 4°$. Pressure and friction coefficient.

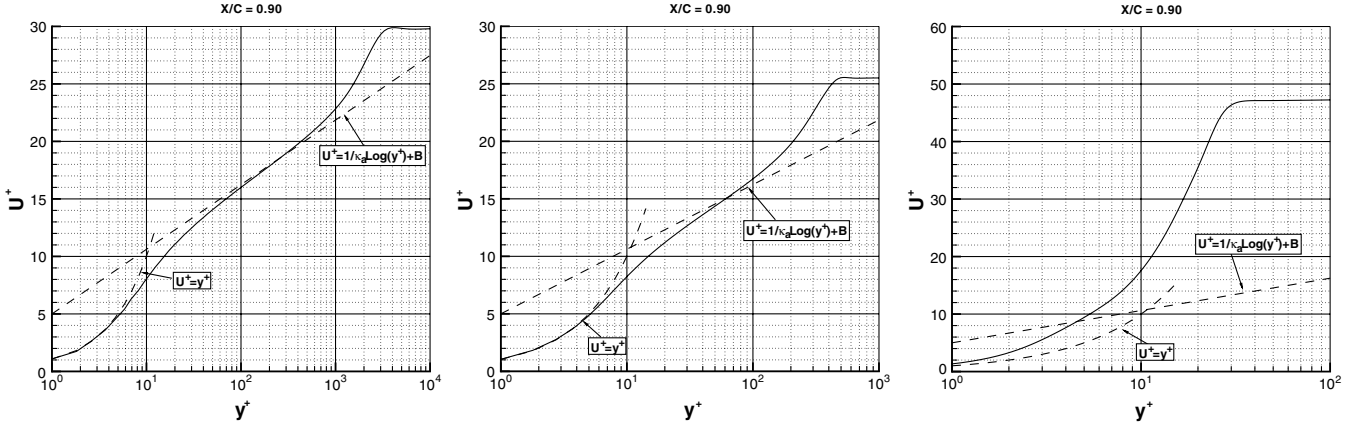

a) Reynolds number = 6.0×10^6 b) Reynolds number = 6.0×10^5 c) Reynolds number = 6.0×10^4

Fig. 9 κ-ω SST. Velocity profiles on the SD 7003 airfoil at three Reynolds numbers, $\alpha = 0°$.

$(u/u_\tau) = (1/\kappa_a) \log y^+ + B$ (with $\kappa_a = 0.41$ and $B = 5.0$) corresponding to the log layer are also shown. The flow at the highest Reynolds number (Fig. 9a) presents a well-defined logarithmic region in a large extent of the boundary layer. At a Reynolds number of 6.0×10^5 (Fig. 9b), the log layer still exists, but both the thickness of the boundary layer and the extension of the logarithmic region are reduced by an order of magnitude. The numerical results well reproduce the theoretical laws of the velocity at both of the Reynolds numbers. On the contrary, at $Re = 6.0 \times 10^4$ (Fig. 9c), the logarithmic region is totally absent in the calculations. The streamwise

velocity has a linear behavior with y^+ for most of the boundary layer but does not follow the viscous law $u^+ = y^+$. The velocity reaches higher values with respect to the other two higher Reynolds numbers.

The eddy viscosity is shown in Fig. 10. The two quantities $a_1\omega$ and $F_2\Omega$ at the denominator of Eq. (5) are also reported as symbols, and their maximum is reported as a solid line. Similar results are obtained at Reynolds numbers 6.0×10^6 (Fig. 10a) and 6.0×10^5 (Fig. 10b). The eddy viscosity is computed as $\mu_t = \rho\kappa/\omega$ in most of the boundary layer. $F_2\Omega$ is greater than $a_1\omega$ in a narrow region close to the zone where μ_t/μ has reached its maximum and starts to decrease. In this region, the eddy viscosity is computed as $\mu_t = a_1\kappa/F_2\Omega$.

At Reynolds number 6.0×10^4 (Fig. 10c), the eddy viscosity μ_t/μ is lower than one for most of the airfoil and greater than one at the station $x/c = 0.90$, where the flow can be considered turbulent. At this location, $F_2\Omega > a_1\omega$ in the region where μ_t/μ is maximum.

The behavior of the blending function F_2 [Eq. (6)] and its arguments [Eqs. (7) and (8)] is presented in Fig. 11. At Reynolds numbers 6.0×10^6 (Fig. 11a) and 6.0×10^5 (Fig. 11b), the F_2, as expected, is computed as a function of the viscous quantity Arg22 in the sublayer and then as a function of the turbulent length scale Arg21 in the remaining part of the boundary layer. At Reynolds number 6.0×10^4 (Fig. 11c), the F_2 shows a large oscillation. Indeed, in the outer part of the boundary layer, it again grows, while it was expected to vanish in order to correctly perform the switch in the eddy viscosity calculation. This unexpected behavior occurs when the viscous argument Arg22 becomes greater than the turbulent argument Arg21.

IV. κ-ω Shear-Stress-Transport Low-Reynolds-Number Modification

The computation of F_2 in the standard SST formulation requires the calculation of the maximum between two arguments [Eq. (6)]. The first one is Arg21 [Eq. (8)], the turbulent length scale divided by the distance from the wall. Arg21 is zero at the body surface, reaches a maximum in the log region, and then vanishes in the upper part of the boundary layer. The second argument is Arg22, which depends on the molecular viscosity μ, the specific dissipation rate ω, and the square of the distance from the body surface. The quantity Arg22 has a constant value close to a solid boundary, since

$$\omega \propto \frac{1}{y^2} \quad \text{as } y \to 0 \tag{9}$$

and behaves as y in the outer part of the boundary layer. Arg22 should be important in the viscous sublayer, while Arg21 should play a role in the logarithmic part of the boundary layer. This occurs at $Re = 6 \times 10^6$ (Fig. 11a) and $Re = 6 \times 10^5$ (Fig. 11b). In these cases, a log region can be clearly discerned in the boundary layer (Fig. 9a and 9b). Arg21 should be small, as the Reynolds number decreases and the log layer tends to disappear, but this is not true at $Re = 6 \times 10^4$. Indeed, the logarithmic region is absent (Fig. 9c), but Arg21 > Arg22 and $F_2 = \tanh(\text{Arg21}^2)$ in a significant part of the boundary layer (Fig. 11c).

A modification is here proposed in order to correctly apply the SST formulation to low-Reynolds-number flows. F_2 is again computed following Eq. (6), but Eq. (7) is modified as

$$\text{Arg}\,2 = \max(1/k_f * \text{Arg21}, \text{Arg22}) \tag{10}$$

with

$$k_f = |\ell_n(k_r/Re)|; \qquad k_r = e^{B/2\kappa_a^2} \tag{11}$$

The coefficient k_f is of an order of magnitude one if $Re \approx 10^6$ and greater than one at lower Reynolds numbers. In this way, Arg21 decreases in case of low-Reynolds-number flows, but the original formulation is recovered for high-Reynolds-number flows.

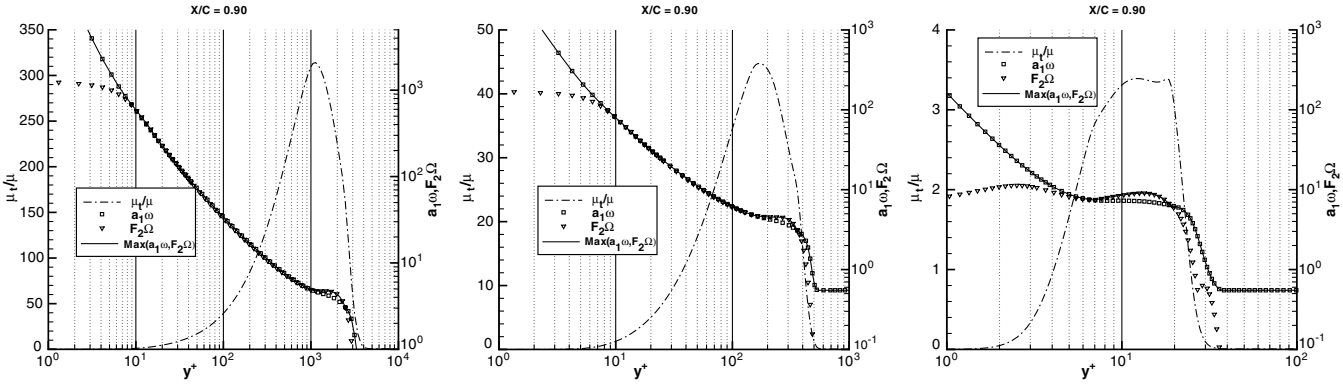

a) Reynolds number = 6.0×10^6 b) Reynolds number = 6.0×10^5 c) Reynolds number = 6.0×10^4

Fig. 10 κ-ω SST. Eddy viscosity profiles on the SD 7003 airfoil at three Reynolds numbers.

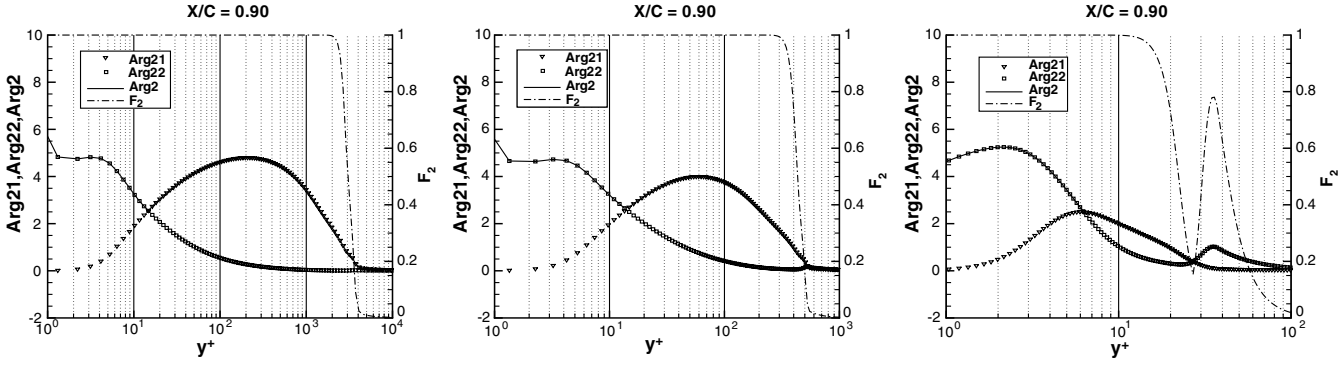

a) Reynolds number = 6.0×10^6 b) Reynolds number = 6.0×10^5 c) Reynolds number = 6.0×10^4

Fig. 11 κ-ω SST. Function F_2 on the SD 7003 airfoil at three Reynolds numbers.

The analysis in the previous section has also highlighted some oscillations of F_2, more clearly as the Reynolds number decreases. As recommended by Menter [8], a limiter for the turbulent specific dissipation in the form

$$\omega \geq \omega_{\lim} = k_\omega \frac{U_\infty}{L_{\text{ref}}}; \qquad k_\omega = 10 \tag{12}$$

has been used in the numerical simulations. This limiter does not properly work as the Reynolds number decreases. It has been updated here as follows:

$$\omega \geq \omega_{\lim} = k_\omega \frac{U_\infty}{L_{\text{ref}}} * k_f \tag{13}$$

The modified model [Eqs. (10), (11), and (13)] is referenced as κ-ω SST low-Reynolds modified (SST-LR) in the following sections.

A. Analysis for Low-Reynolds-Number Flows

The simulations of the flow around the SD 7003 airfoil at $\alpha = 0°$ and the Reynolds numbers 6×10^6, 6×10^5, and 6×10^4 have been repeated by using the κ-ω SST-LR modification.

The velocity profiles are presented in Fig. 12. There are negligible differences with the velocities provided by the κ-ω SST at Reynolds numbers 6×10^6 and 6×10^5. Large differences are instead seen at Reynolds number 6×10^4. Indeed, a viscous region is now clearly identified in the boundary layer. The velocity profiles follow the linear law $u^+ = y^+$ very well. The levels of u^+ remain of the same order of magnitude as at the higher Reynolds numbers. It is interesting to compare Figs. 9c and 12c. The κ-ω SST-LR provides a boundary-layer profile with a small visible log region, which implies a significant turbulence.

The eddy viscosity is shown in Fig. 13. The results obtained by the κ-ω SST-LR model at Reynolds number 6×10^6 (Fig. 13a) present the same behavior as the μ_t/μ provided by the κ-ω SST, in terms of either maximum value, and zone where this maximum is attained. At Reynolds number 6×10^5 (Fig. 13b), the κ-ω SST-LR returns a flow slightly more turbulent than the standard SST. The eddy viscosity behavior after the maximum is slightly more irregular than the standard SST. At Reynolds number 6×10^4 (Fig. 13c), the κ-ω SST-LR provides a turbulent flow ($\mu_t/\mu \geq 1$), also upstream the station $x/c = 0.90$. The eddy viscosity is computed as $\mu_t = \rho\kappa/\omega$ in the entire boundary layer. The new limiter equation (13) increases the value of $a_1\omega$ significantly at the edge of the boundary layer.

Figure 14 shows the function F_2 computed by Eqs. (6), (10), and (11). There are not significant differences between the results obtained by the κ-ω SST-LR and SST at all three Reynolds numbers. The F_2 obtained by the κ-ω SST-LR has the same behavior and goes to zero in the same zone of the boundary layer as the results provided by the κ-ω SST (Fig. 11). The oscillation in the F_2 is largely reduced but still present. F_2 depends on Arg22 close to the airfoil surface and is $F_2 = \tanh(\text{Arg}21^2)$ in the log-layer zone. At Reynolds number 6×10^4, $F_2 = \tanh(\text{Arg}22^2)$, except in a very narrow zone. This is consistent with the fact that the κ-ω SST-LR provides, at $Re = 6 \times 10^4$ and $x/c = 0.90$, a turbulent solution with a logarithmic region in the boundary layer.

In conclusion, the κ-ω SST-LR has returned the same results as the κ-ω SST model at a high Reynolds number and improved the results at a low Reynolds number. In particular, at Reynolds number 6×10^4,

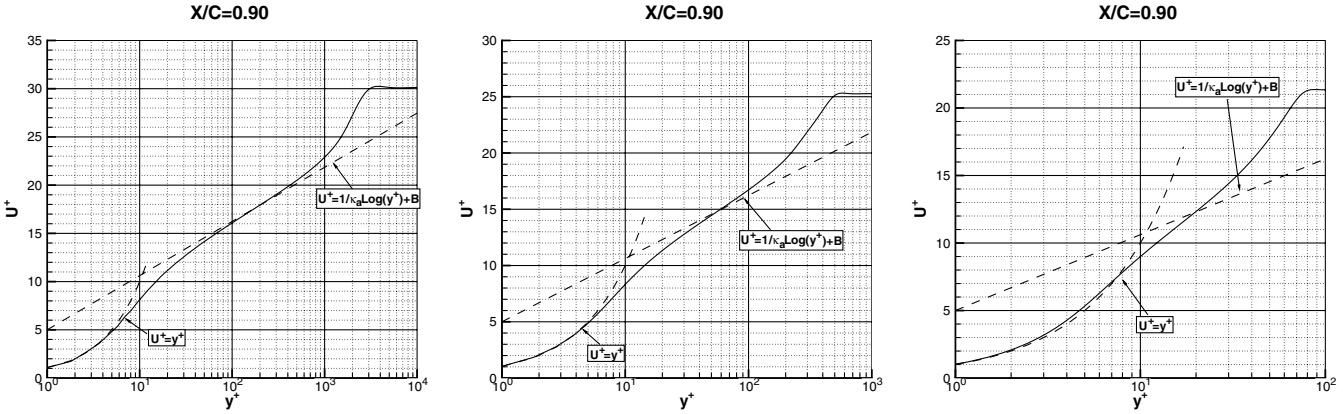

a) Reynolds number = 6.0×10^6 **b) Reynolds number = 6.0×10^5** **c) Reynolds number = 6.0×10^4**

Fig. 12 κ-ω SST-LR. Velocity profiles on the SD 7003 airfoil at three Reynolds numbers, $\alpha = 0°$.

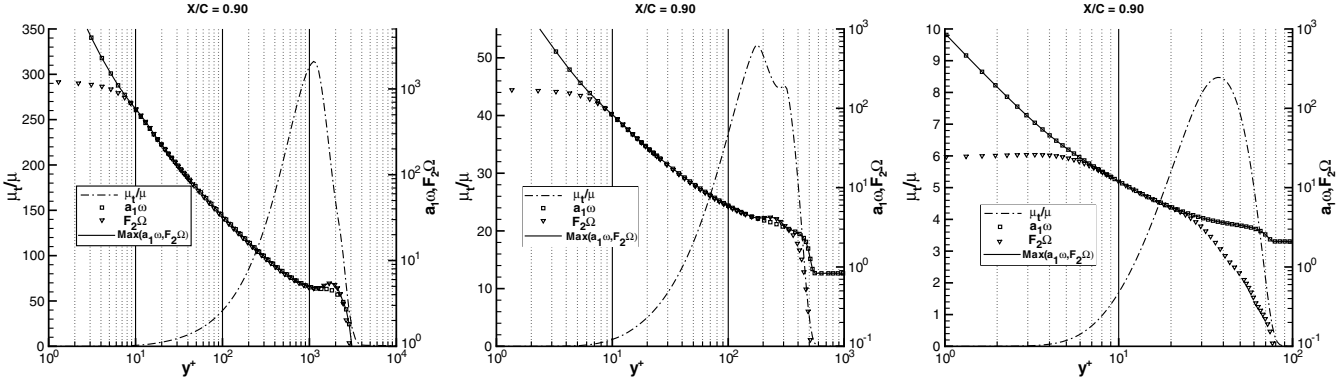

a) Reynolds number = 6.0×10^6 **b) Reynolds number = 6.0×10^5** **c) Reynolds number = 6.0×10^4**

Fig. 13 κ-ω SST-LR. Eddy viscosity profiles on the SD 7003 airfoil at three Reynolds numbers.

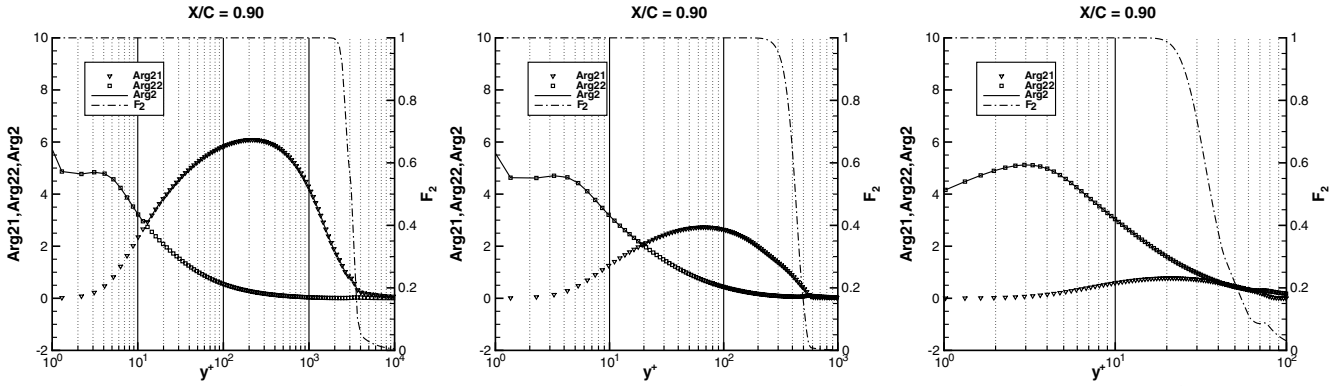

a) Reynolds number = 6.0×10^6 b) Reynolds number = 6.0×10^5 c) Reynolds number = 6.0×10^4

Fig. 14 κ-ω SST-LR. Function F_2 on the SD 7003 airfoil at three Reynolds numbers.

the flow presents a well-defined viscous region and a developing turbulent logarithmic zone.

The κ-ω SST-LR model has been applied to compute the flow at $\alpha = 4°$ and Reynolds number 6×10^4 around the SD 7003 airfoil. The freestream values of the turbulence are lowered [$(\mu_t/\mu)_\infty = 1 \times 10^{-9}$ and $(\sqrt{\kappa}/U)_\infty = 10^{-6}$] in such a way to obtain a LSB. The model has been employed with and without the transition imposed (same numerical input as previous tests with the standard formulation).

The new, and some previous, results are presented together in Fig. 15. In the case of the simulation with the transition point fixed, the results obtained by the κ-ω SST-LR model are significantly improved with respect to the standard SST. The κ-ω SST-LR model has returned a flow more turbulent than the standard SST. This has allowed the reattachment of the flow and a pressure recovery in a far better agreement with LES results. The results are also slightly improved with respect to the κ-ω BSL, with a better agreement of the reattachment point. The streamlines and the contour map of the module of the velocity achieved by the κ-ω SST-LR are shown in Fig. 16. The structure of a LSB (Fig. 2) is well resembled. The height and the length of the bubble are in good agreement with LES results (Fig. 5b) and improved with respect to the κ-ω SST model (Fig. 5a).

In the case of simulation without specification of the transition point, the modifications of the results are not so dramatic; in particular, the agreement of the reattachment point with LES results remains poor.

These results highlight the need of a proper prediction method for a correct simulation of low-Reynolds-number flows. Recently, promising results have been obtained by introducing standard transition prediction methods in the RANS time iterations [6,30]. A possible practical alternative can be the following. First, the presence of LSBs can be detected by a simulation with low values of freestream turbulence. Then, the results can be improved by imposing the transition location. A reasonable point is downstream of the X/C, where the friction coefficient is minimum.

The flow at $\alpha = 6°$ has been computed by this strategy and by applying the κ-ω SST and SST-LR turbulence models. The results are shown in Fig. 17. The transition location is fixed 10% downstream of the point of minimum C_F. The pressure and friction coefficients achieved by the κ-ω SST-LR in the case of prescribed transition are in very good agreement with the LES data. The κ-ω SST model returns a poor result, as for the flow, at $\alpha = 4°$.

The same strategy has also been applied to the flow at $\alpha = 8$ and 9°, and the same kind of result has been obtained.

B. Drag Polar of the SD 7003 Airfoil

The drag polar of the SD 7003 airfoil at Reynolds number 6.0×10^4 has been computed by LES and by RANS with the κ-ω SST and SST-LR models.

The lift and drag coefficients are compared (Fig. 18) to three sets of experimental data and to the numerical results obtained by the ILES approach [14]. The measurements taken from Selig et al. [31] at the University of Princeton in 1989, from Selig et al. [32] at the University of Illinois in 1996, and from Ol et al. [4] at the horizontal free-surface wind tunnel (HFWT) of the U.S. Air Force Research Laboratory in 2005 are considered.

The lift curve shows that the κ-ω SST model provides a stall, anticipated with respect to all the other sets of data. The κ-ω SST-LR model follows the experimental and ILES data very well. The largest differences are with the HFWT data and are always lower than 5%. The LES data slightly overpredict the ILES (6% at $\alpha = 6$) and

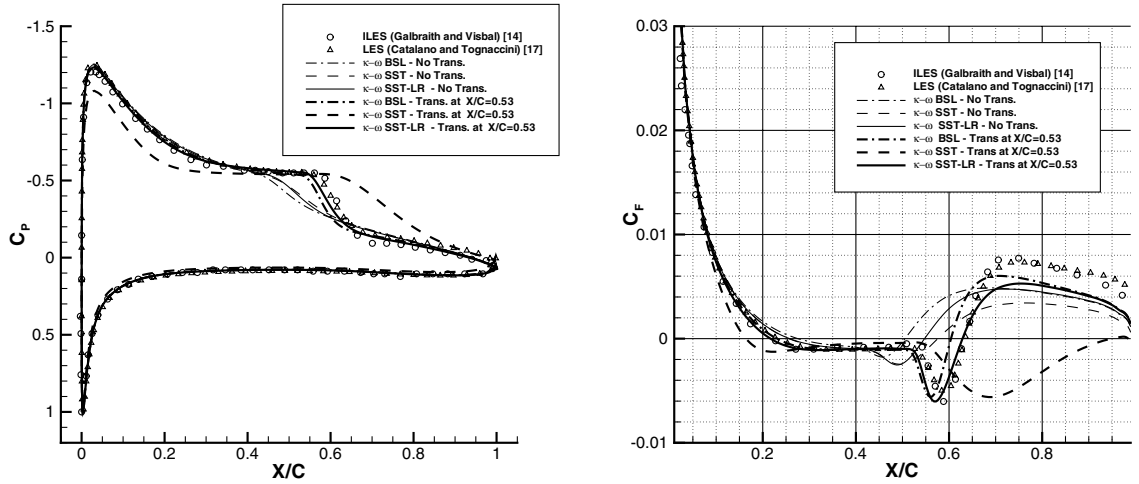

a) Pressure coefficient b) Friction coefficient

Fig. 15 SD 7003 Airfoil, $Re = 6 \times 10^4$, $\alpha = 4°$. Pressure and friction coefficient.

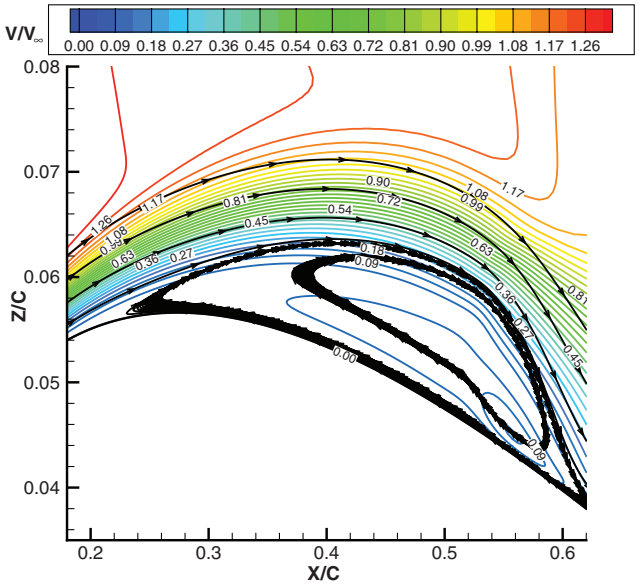

Fig. 16 SD 7003 airfoil, $Re = 6.0 \times 10^4$, $\alpha = 4°$. RANS κ-ω SST-LR, transition fixed ($x_{tr}/c = 0.53$): structure of the laminar bubble.

experimental data (10% with respect to HFWT, 2% with respect to Selig 96, and 3% with respect to Selig 89 at $\alpha = 6$).

All the drag coefficients, computed by a near-field method, overpredict the experimental measurements (Fig. 18b). The LESs are in good agreement between them. The largest difference is about 8% at $\alpha = 6$. The RANS results are in between the LES and the experiments.

The comparison between the RANS (with transition not prescribed) and the LES is acceptable only for low angles of attack. The C_D and C_L obtained by the κ-ω SST-LR with an imposed transition point (even if with a very rough criterion) are also shown in Fig. 18. The agreement with the aerodynamic coefficients provided by the LESs improves.

C. Analysis for Transonic Flows

To verify that SST formulation is recovered for transonic flows at high Reynolds numbers, the κ-ω SST-LR turbulence model is applied to the RAE M2155 wing placed in a wind tunnel. This is a transonic benchmark [33] for which the κ-ω SST model has provided remarkable results [18]. For the case 2 condition: 1) the Mach number is 0.806, 2) the Reynolds number is 4.1×10^6, and 3) $\alpha = 2.50°$ is characterized by a quite complex shock topology [33]. The flow on the upper surface of the wing is characterized by a triple shock wave system, from the root to about the 50% of the span,

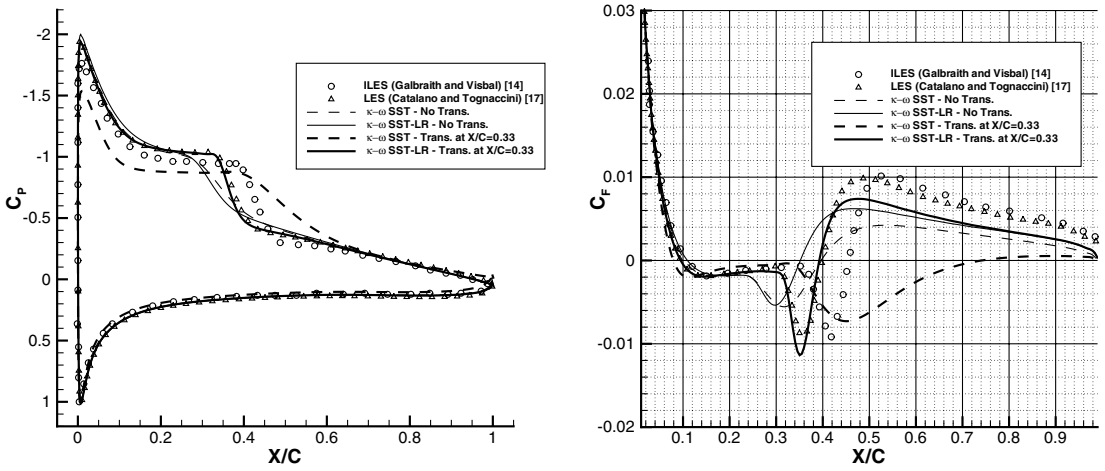

a) Pressure coefficient **b) Friction coefficient**

Fig. 17 SD 7003 airfoil, $Re = 6 \times 10^4$, $\alpha = 6°$. Pressure and friction coefficient.

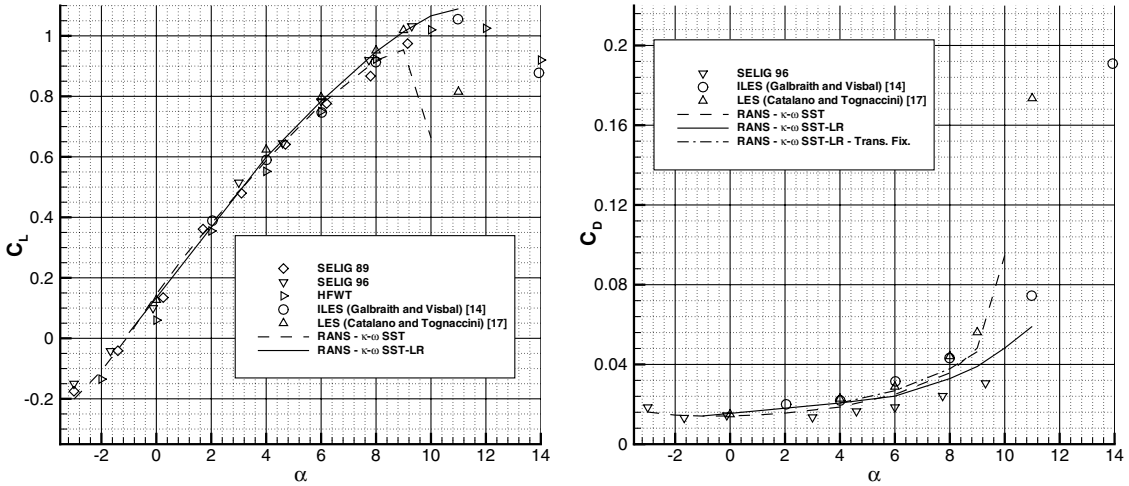

a) Lift coefficient **b) Drag coefficient**

Fig. 18 SD 7003 airfoil: drag polar at $Re = 6.0 \times 10^4$.

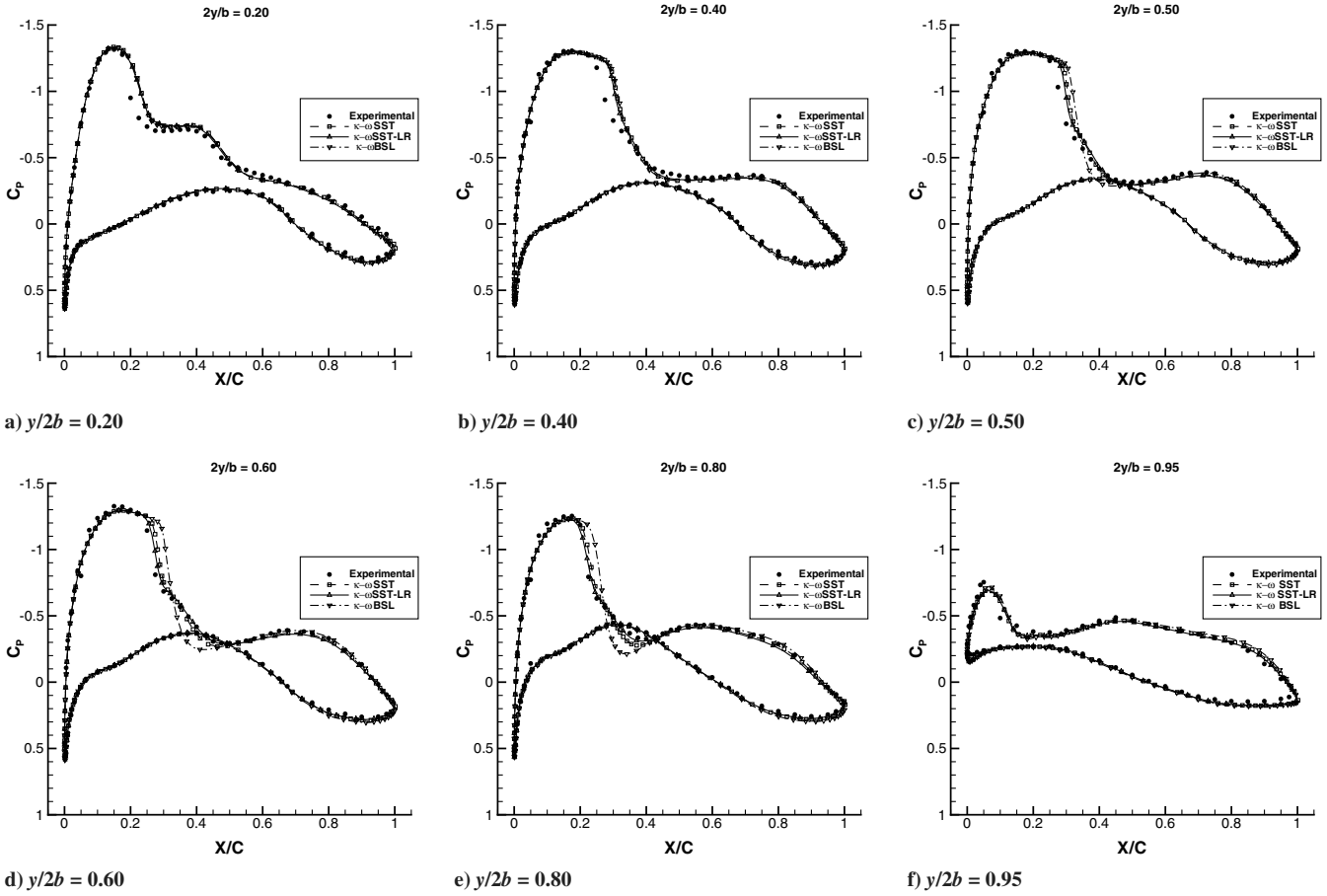

a) $y/2b = 0.20$ b) $y/2b = 0.40$ c) $y/2b = 0.50$

d) $y/2b = 0.60$ e) $y/2b = 0.80$ f) $y/2b = 0.95$

Fig. 19 Pressure coefficients over the RAE M2155 wing.

and by a single shock wave, from about 50% to the tip. Inboard the 50% span, changes in the flow direction occur in the region of the forward leg of the triple shock wave system and in the trailing-edge zone, but without flow separation. The flow separation starts where the three shock waves join together and ends at about 90% of the span. The separation extends for about 10% of the local chord.

A mesh with 35 blocks and about 1.2×10^6 cells has been employed. The κ-ω SST, SST-LR, and BSL turbulence models are applied.

The results are shown in terms of pressure coefficients at several stations along the span in Fig. 19. At the inboard spanwise stations, the interaction between the shock wave system and the boundary layer is not very strong, and the three κ-ω models present the same pressure coefficients. At the stations where the shock boundary-layer interaction becomes stronger and the flow separates, the κ-ω SST-LR provides the same results as the standard SST model and follows the experimental data better than the BSL model.

V. Conclusions

The capability of a turbulence model to return a LSB and the application of the κ-ω SST model to flows at low Reynolds numbers have been investigated. The incompressible flow at Reynolds number 6×10^4 around the SD 7003 airfoil has been considered. LESs have also been performed and used as a reference for the RANS results.

LSBs have been found by the Spalart–Allmaras and the κ-ω SST turbulence models. The simulations have been performed using very low values of the freestream turbulence, without an a priori knowledge of the laminar-turbulent transition, and by prescribing the transition location as retrieved by the LES data. A satisfactory prediction of the flow characteristics in the dead-air region of the bubble is obtained. On the contrary, a poor agreement has been provided by RANS with respect to LES in the zone of pressure recovery. These discrepancies are essentially due to a too-low level of turbulence in the bubble.

The behavior of the κ-ω SST turbulence model has been investigated in detail. Simulations of the flow around the SD 7003 airfoil at Reynolds numbers 6×10^4, 6×10^5, and 6×10^6 have been performed. This model did not correctly predict the viscous and logarithmic regions of the boundary layer at the lowest Reynolds number. However, it has been shown that this is related to the implementation at low Reynolds numbers rather than to an intrinsic design limit of the model. Indeed, a modification has been proposed (κ-ω SST-LR turbulence model). The modified model has provided a correct simulation of the viscous sublayer and logarithmic region in the tests performed at $Re = 6.0 \times 10^4$. The LSB arising on the SD 7003 airfoil is well captured, and the results of the RANS simulations are in excellent agreement with the LES data when the transition location is specified to agree with LES a priori.

The proposed modification uses nonlocal quantities: in particular, the Reynolds number of the flow. This aspect can be a problem in some analyses: for instance, for multielement airfoils. The authors are still looking for a possible alternative based on local quantities.

Finally, the high-Reynolds-number performances of the modified model do not deteriorate with respect to the standard κ-ω SST, as shown by the transonic test around the RAE M2155 wing.

References

[1] Howard, R. J. A., Alam, M., and Sandham, N. D., "Two-Equations Turbulence Modelling of a Transitional Separation Bubble," *Flow, Turbulence and Combustion*, Vol. 63, Nos. 1–4, 2000, pp. 175–191. doi:10.1023/A:1009992406036

[2] Kalitzin, G., Gould, A., and Benton, J., "Application of Two-Equation Turbulence Models to Aircraft Design," 34th AIAA Aerospace Sciences Meeting and Exhibit, AIAA Paper 96-0327, 1996.

[3] Wilcox, D. C., *Turbulence Modeling for CFD*, DCW Industries, Los Angeles, CA, 1994.

[4] Ol, M. V., McAuliffe, B. R., Hanff, E. S., Scholz, U., and Kalher, C., "Comparison of Laminar Separation Bubble Measurements on a Low Reynolds Number Airfoil in Three Facilities," 135th AIAA Fluid Dynamics Conference, AIAA Paper 2005-5149, June 2005.

[5] Windte, J., Scholz, U., and Radespiel, R., "Validation of RANS Simulation of Laminar Separation Bubbles on Airfoils," *Aerospace Science and Technology*, Vol. 10, No. 6, 2006, pp. 484–494. doi:10.1016/j.ast.2006.03.008

[6] Radespiel, R., Windte, J., and Scholz, U., "Numerical and Experimental Flow Analysis of Moving Airfoils with Laminar Separation Bubbles," 44th AIAA Aerospace Sciences Meeting and Exhibit, AIAA Paper 2006-0501, Jan. 2006.

[7] Yuan, W., Khalid, M., Windte, J., Scholz, U., and Radespiel, R., "An Investigation of Low-Reynolds-Number Flows Past Airfoils," 23rd AIAA Applied Aerodynamics Conference, AIAA Paper 2005-4607, June 2005.

[8] Menter, F. R., "Two-Equation Eddy Viscosity Turbulence Models for Engineering Applications," *AIAA Journal*, Vol. 32, No. 8, 1994, pp. 1598–1695. doi:10.2514/3.12149

[9] Wallin, S., and Johansson, A., "An Explicit Algebraic Reynolds Stress Model for Incompressible and Compressible Turbulent Flows," *Journal of Fluid Mechanics*, Vol. 403, 2000, pp. 89–132. doi:10.1017/S0022112099007004

[10] Tang, L., "RANS Simulation of Low-Reynolds-Number Airfoil Aerodynamics," 44th AIAA Aerospace Science Meetinf and Exhibit, AIAA Paper 2006-0249, Jan. 2006.

[11] Jones, W. P., and Launder, B. E., "The Prediction of Laminarization with a Two-Equation Model for Turbulence," *International Journal of Heat and Mass Transfer*, Vol. 15, No. 2, 1972, pp. 301–314. doi:10.1016/0017-9310(72)90076-2

[12] Ferziger, J. H., and Peric, M., *Computational Methods for Fluid Dynamics*, Springer–Verlag, Berlin, 1996.

[13] Lenormand, E., Saguat, P., Phuoc, L., and Comte, P., "Subgrid-Scale Models for Large Eddy Simulation of Compressible Wall Bounded Flows," *AIAA Journal*, Vol. 38, No. 8, 2000, pp. 1340–1350. doi:10.2514/2.1133

[14] Galbraith, M. C., and Visbal, M. R., "Implicit Large Eddy Simulation of Low Reynolds Number Flow past the SD 7003 Airfoil," 46th AIAA Aerospace Sciences Meeting and Exhibit, AIAA Paper 2008-225, Jan. 2008.

[15] Rumsey, C. L., and Spalart, P. R., "Turbulence Model Behavior in Low Reynolds Number Regions of Aerodynamic Flow Fields," *AIAA Journal*, Vol. 47, No. 4, 2009, pp. 982–993. doi:10.2514/1.39947

[16] Spalart, P. R., and Rumsey, C. L., "Effective Inflow Conditions for Turbulence Models in Aerodynamic Calculations," *AIAA Journal*, Vol. 45, No. 10, 2007, pp. 2544–2553. doi:10.2514/1.29373

[17] Catalano, P., and Tognaccini, R., "Influence of Free-Stream Turbulence on Simulations of Laminar Separation Bubbles," 47th AIAA Aerospace Sciences Meeting and Exhibit, AIAA Paper 2009-1471, Jan. 2009.

[18] Catalano, P., and Amato, M., "An Evaluation of RANS Turbulence Modelling for Aerodynamic Applications," *Aerospace Science and Technology*, Vol. 7, No. 7, 2003, pp. 493–509. doi:10.1016/S1270-9638(03)00061-0

[19] Marongiu, C., Catalano, P., Amato, M., and Iaccarino, G., "U-ZEN : A Computational Tool Solving U-RANS Equations for Industrial Unsteady Applications," 34th AIAA Fluid Dynamics Conference, AIAA Paper 2004-2345, 2004.

[20] Jameson, A., "Time Dependent Calculations Using Multigrid with Application to Unsteady Flows past Airfoils and Wings," AIAA Paper 1991-1596, June 1991.

[21] Catalano, P., and Amato, M., "Assessment of κ-ω Turbulence Modeling in the CIRA Flow Solver ZEN," *ECCOMAS 2001 Conference* [CD-ROM], Inst. of Mathematics and its Applications, Univ. of Wales, Swansea, Wales, 4–7 Sept. 2001.

[22] Amato, M., and Catalano, P., "Non Linear κ-ε Turbulence Modeling for Industrial Applications," *ICAS 2000 Congress* [CD-ROM], International Council of the Aeronautical Sciences, Les Mureaux, France, 2000.

[23] Kim, J., and Moin, P., "Application of a Fractional Step Method to Incompressible Navier–Stokes Equations," *Journal of Computational Physics*, Vol. 59, No. 2, 1985, pp. 308–323. doi:10.1016/0021-9991(85)90148-2

[24] Germano, M., Piomelli, U., Moin, P., and Cabot, W. H., "A Dynamic Subgrid-Scale Eddy Viscosity Model," *Physics of Fluids, A, Fluid Dynamics*, Vol. 3, No. 7, 1991, pp. 1760–1765. doi:10.1063/1.857955

[25] Lilly, D. K., "A Proposed Modification of the Germano Subgrid Scale Closure Method," *Physics of Fluids, A, Fluid Dynamics*, Vol. 4, 1992, pp. 633–635. doi:10.1063/1.858280

[26] Kok, J., "Resolving the Dependence on Free-Stream Values for the κ-ω Turbulence Model," *AIAA Journal*, Vol. 38, No. 7, 2000, pp. 1292–1295. doi:10.2514/2.1101

[27] Horton, H. P., "Laminar Separation in Two and Three-Dimensional Incompressible Flow," Ph.D. Thesis, Univ. of London, London, 1968.

[28] Marxen, O., Lang, M., Rist, U., and Wagner, S., "A Combined Numerical/Experimental Study of Unsteady Phenomena in a Laminar Separation Bubble," *Flow, Turbulence and Combustion*, Vol. 71, Nos. 1–4, 2003, pp. 133–146. doi:10.1023/B:APPL.0000014928.69394.50

[29] Lang, M., Rist, U., and Wagner, S., "Investigation on Controlled Transition Development in a Laminar Separation Bubble by Means of LDA and PIV," *Experiments in Fluids*, Vol. 36, No. 1, 2004, pp. 43–52. doi:10.1007/s00348-003-0625-x

[30] Catalano, P., Iuliano, E., Donelli, R., and Paniza, A., "A Numerical Procedure for Predicting Transition in a RANS Environment," *XX Congresso Nazionale AIDAA* [CD-ROM], Assoc. Italiana di Aeronautica ed Astronautica, Milan, 2009.

[31] Selig, M. S., Donovan, J. F., and Fraser, D. B., "Airfoils at Low Speeds," *Soartech 8*, edited by H. A. Stokely, Soartech Aero Publ., Virginia Beach, VA, 1989.

[32] Selig, M. S., Guglielmo, J. J., Groeren, A. P., and Giguere, P., *Summary of Low-Speed Airfoil Data*, edited by H. A. Stokely, Soartech Aero Publ., Virginia Beach, VA, 1995.

[33] Firmin, M. C. P., and McDonald, M. A., "Measurements of the Flow over a Low Aspect-Ratio Wing in the Mach Number Range 0.6 to 0.87 for the Purpose of Validation of Computational Methods," Defence Research Agency TR 92016, Worcestershire, U.K., 1992.

S. Fu
Associate Editor